



# Structure of *N*-myristoyltransferase from *Aspergillus fumigatus*

Takashi Shimada,\* Makoto Suzuki and Shin-ichi Katakura

Drug Discovery and Biomedical Technology Unit, Daiichi Sankyo RD Novare Co. Ltd, 1-16-13 Kita-kasai, Edogawa-ku, Tokyo 134-8630, Japan. \*Correspondence e-mail: shimada.takashi.zj@rdn.daiichisankyo.co.jp

Received 21 September 2014

Accepted 9 January 2015

Edited by Q. Hao, University of Hong Kong

**Keywords:** *N*-myristoyltransferase; *Aspergillus fumigatus*.

**PDB reference:** *N*-myristoyltransferase complexed with a synthetic inhibitor, 4qbj

**Supporting information:** this article has supporting information at journals.iucr.org/d

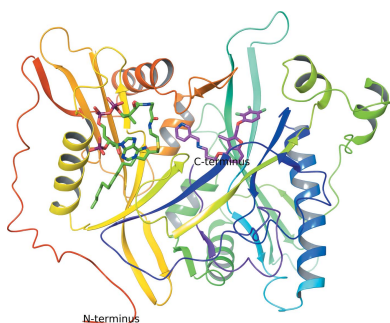
*N*-Myristoyltransferase (NMT) is an enzyme which translocates the 14-carbon saturated fatty acid myristate from myristoyl-CoA to the N-terminal glycine of substrate peptides. This myristoylation process is involved in protein modification in various eukaryotes, including animals and fungi. Furthermore, this enzyme has been shown to be essential to the growth of various species, such as *Saccharomyces cerevisiae*, which indicates that NMT is an attractive target for the development of a novel antifungal drug. In this study, the crystal structure of a ternary complex of NMT from *Aspergillus fumigatus* with *S*-(2-oxo)pentadecyl-CoA, a myristoyl-CoA analogue cofactor, and a synthetic inhibitor is reported at a resolution of 2.1 Å. The results advance the understanding of the specificity of NMT inhibitors and provide valuable information for structure-based drug design.

## 1. Introduction

*Aspergillus fumigatus* is a saprophytic filamentous fungus that causes invasive mycosis. Two types of mycosis are known: superficial infection and subcutaneous infection. Subcutaneous infection includes systemic infection, which sometimes has a lethal effect on humans. This type of infection is particular to the cases of cancer patients, AIDS patients and haematopoietic stem-cell transplant recipients, whose immune levels are low (Latgé, 1999). Therefore, an effective way of treating mycosis is desired. Other than *A. fumigatus*, other fungi that are known to cause systemic infection in humans include *Candida albicans* and *Cryptococcus neoformans* (Chen & Rodriguez, 2003). Infections with *C. albicans* are the major cause of mycosis; however, infections with the *Aspergillus* genus, especially *A. fumigatus*, have been reported to be a second major cause (Pfaller *et al.*, 2006).

Several drugs for the treatment of *Aspergillus* infections are available, such as polyenes (amphotericin B *etc.*), azoles (fluconazol, miconazol *etc.*) and echinocandins (caspofungin *etc.*) (Howard *et al.*, 2010; Snelders *et al.*, 2011). Each drug has a unique inhibition mechanism. For example, polyenes have a direct effect on the cell membrane of fungi, azoles inhibit the synthesis pathway of ergosterol, and echinocandins directly inhibit 1,3- $\beta$ -D-glucane synthetase. Currently, voriconazole from Pfizer is widely used for the treatment of invasive *Aspergillus* infections and amphotericin B-resistant infections (Herbrecht *et al.*, 2002). However, each drug also has its own problems, such as narrowness of the antifungal spectrum, side effects and acquired resistance. Therefore, a novel drug for *Aspergillus* infections with a new inhibition mechanism and high safety is required.

Peptide *N*-myristoyltransferase (NMT; glycylpeptide *N*-tetradecanoyltransferase or myristoyl-CoA:protein *N*-myristoyltransferase) catalyzes a translocation reaction of the



myristoyl group to the N-terminal glycine of a peptide (Rudnick *et al.*, 1993; Johnson *et al.*, 1994; Knoll *et al.*, 1995; Boutin, 1997). This reaction is an irreversible process and can be found in translational and post-translational reactions in various eukaryotes, including animals and fungi. Inhibition of this reaction is known to inhibit the growth of some fungi (Nakayama *et al.*, 2000; Masubuchi *et al.*, 2001, 2003; Ebiike *et al.*, 2002; Kawasaki *et al.*, 2003; Snelders *et al.*, 2011; Rackham *et al.*, 2013). Thus, this enzyme has been considered to have potential as a target for novel antifungal drugs. On the other hand, the selective inhibition of fungal NMTs is essential for the development of an NMT inhibitor as an antifungal drug because humans possess a homologue of NMT. Currently, several scaffolds have been reported as NMT inhibitors for antifungal treatments (Zhao & Ma, 2014), such as imidazoles (Devadas *et al.*, 1995), benzofurans (Masubuchi *et al.*, 2001), benzothiazoles (Ebara *et al.*, 2005), isoquinolines (Siwek *et al.*, 2012) and dihydrobenzofurans (Laczkowski *et al.*, 2013). Some of them showed antifungal efficacy in an animal model (Kawasaki *et al.*, 2003).

Ro-09-4879 (Fig. 1), a synthetic inhibitor of *C. albicans* NMT (CaNMT), strongly inhibits the enzyme (with an  $IC_{50}$  of  $0.0057 \mu M$ ) and the growth of the fungus (with an MIC of  $0.11 \mu M$ ) in a substrate peptide-competitive manner (Ebiike *et al.*, 2002; Kawasaki *et al.*, 2003; Masubuchi *et al.*, 2003). However, the inhibitory activity of this compound against *A. fumigatus* NMT (AfNMT) is quite low ( $IC_{50}$  of  $1.0 \mu M$ ; unpublished data) and its antifungal activity against *A. fumigatus* is also weak (MIC of  $55 \mu M$ ; Masubuchi *et al.*, 2003), presumably owing to the lack of high sequence identity (48%) between AfNMT and CaNMT. When we started the structure-based drug-discovery project for a low-molecular-weight inhibitor with anti-*A. fumigatus* activity, we decided to solve the crystal structure of Ro-09-4879 complexed with AfNMT and *S*-(2-oxo)pentadecyl-CoA (an analogue of the cofactor myristoyl-CoA; Fig. 1) as a starting compound.

Crystal structures of NMT from many species have been solved, such as human (PDB entries 1rxt, 3iu1, 3iu2, 3iwe and 3jtk; J. Yang, Y. Wang, G. Frey, R. H. Abeles, G. A. Petsko & D. Ringe, unpublished work; Structural Genomics Consortium, unpublished work), *Saccharomyces cerevisiae* (PDB entries 1iic, 1iid, 2nmt, 2p6e, 2p6f and 2p6g; Bhatnagar *et al.*, 1998; Farazi *et al.*, 2001; Wu *et al.*, 2007), *C. albicans* (PDB entries 1iyk, 1iyl and 1nmt; Weston *et al.*, 1998; Sogabe *et al.*,

2002), *Leishmania donovani* (PDB entry 2wu; Brannigan *et al.*, 2010), *L. major* (PDB entries 2wsa, 3h5z, 4a30, 4cgl, 4cgm, 4cgn, 4cgo and 4cgp; Frearson *et al.*, 2010; Brand *et al.*, 2012; Brannigan *et al.*, 2014), *Plasmodium vivax* (PDB entries 2ync, 2ynd, 2yne, 4a95, 4b10, 4b11, 4b12, 4b13, 4b14, 4bbh, 4cae and 4caf; Goncalves *et al.*, 2012; Yu *et al.*, 2012; Rackham *et al.*, 2013; Wright *et al.*, 2014) and *A. fumigatus* (PDB entries 4cav, 4caw and 4cax; W. Fang, D. A. Robinson, O. G. Raimi, D. E. Blair, J. Harrison, G. F. Ruda, D. E. A. Lockhart, L. S. Torrie, P. G. Wyatt, I. H. Gilbert & D. M. F. van Aalten, unpublished work). Overall, the folding pattern is common to all of these species; however, the amino-acid sequences are not completely conserved (Fig. 2). Furthermore, it is known that in some cases structured waters play an important role in molecular recognition. Therefore, it is necessary to obtain the structures of complexes with inhibitors for each species at high resolution to confirm the mechanism behind the specificity of the compound.

In this study, we successfully solved the crystal structure at the high resolution of 2.1 Å. Our structure now provides molecular details of the interactions between AfNMT, *S*-(2-oxo)pentadecyl-CoA and the inhibitor, including water-mediated hydrogen bonds, enabling us to understand the specificity of inhibitors of NMTs among various species and to take a structure-based drug-discovery approach to obtain a novel inhibitor of AfNMT.

## 2. Materials and methods

### 2.1. Synthesis of Ro-09-4879

Ro-09-4879 was synthesized as reported by Ebiike *et al.* (2002).

### 2.2. Synthesis of *S*-(2-oxo)pentadecyl-CoA

*S*-(2-Oxo)pentadecyl-CoA was synthesized as reported by Brannigan *et al.* (2010).

### 2.3. Expression and purification of AfNMT

The plasmid pET-28a (Novagen) containing the AfNMT (101–492) gene fused to a His<sub>6</sub> tag with a thrombin cleavage site between AfNMT and the His<sub>6</sub> tag at the N-terminus was transformed into *Escherichia coli* strain BL21(DE3). The *E. coli* cells were grown statically at 310 K overnight in 35 ml

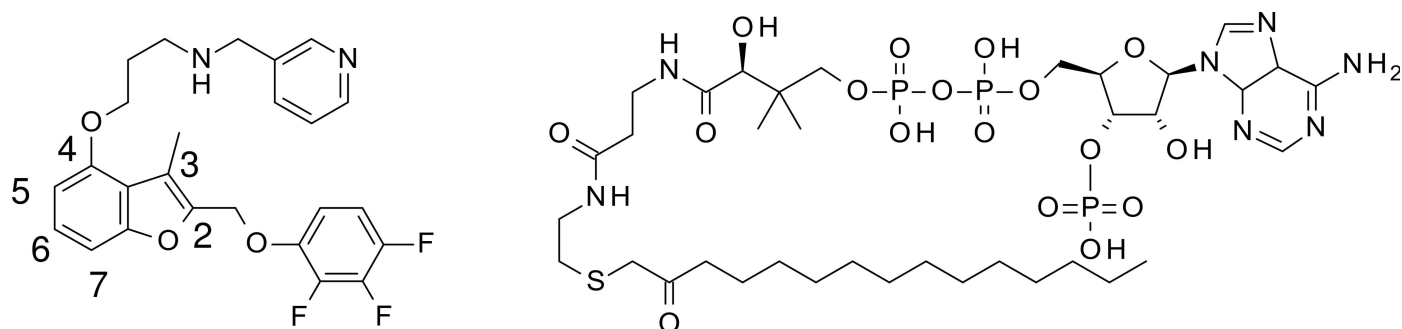


**Figure 1**  
Chemical structures of Ro-09-4879 (left) and *S*-(2-oxo)pentadecyl-CoA, an analogue of the cofactor myristoyl-CoA (right).

LB medium containing 50 µg ml<sup>-1</sup> kanamycin. 2 ml of the overnight culture (*A*<sub>600</sub> = 0.62) was inoculated into 16 bottles containing 100 ml LB-kanamycin medium and then grown at 310 K with shaking at 140 rev min<sup>-1</sup> to an *A*<sub>600</sub> of 1.84 after 4 h; protein expression was then induced with 1 mM IPTG. After 2 h of expression, the cells were collected by centrifugation at 6000 rev min<sup>-1</sup> for 2 min, suspended in 160 ml PBS and centrifuged again. The cell pellets were suspended in 80 ml lysis buffer consisting of 100 mM Tris pH 7.8, 300 mM NaCl, 20 mM imidazole, 2 mM PMSF and cComplete EDTA-free tablets (one tablet per 50 ml; Roche Applied Science). After an equal volume of 1 mg ml<sup>-1</sup> lysozyme/deionized water had been added, the lysis buffer was kept on ice for 30 min. The cells were sonicated at 277 K for 30 s three times and centrifuged at 277 K at 20 000 rev min<sup>-1</sup> for 30 min.

The lysis extract was first loaded onto an Ni-NTA column (Qiagen) and washed with wash buffer (50 mM Tris pH 7.8, 150 mM NaCl). The AfNMT protein fraction was then eluted with elution buffer (50 mM Tris pH 7.8, 150 mM NaCl, 500 mM imidazole). This eluted fraction was dialyzed with 1 l dialysis buffer (50 mM HEPES pH 7.4, 1 mM EDTA, 1 mM DTT) twice. Finally, this protein solution was concentrated to 4.5 ml (2.6 mg ml<sup>-1</sup>).

21 µl 1 M calcium chloride solution was added to 4 ml protein solution and was pre-incubated at 308 K for 10 min. To remove the His<sub>6</sub> tag from AfNMT, human thrombin powder [1:130(w/w), Sigma] was added to this protein solution, which was then incubated at 308 K for 90 min. After 1 ml benzamidine Sepharose (Amersham Biosciences) had been added, the solution was stirred gently at 277 K for 2 h to remove the thrombin. The solution was centrifuged and filtrated with a 0.22 µm filter to remove benzamidine Sepharose gel and was then mixed with an equal volume of equilibrium buffer (50 mM HEPES pH 7.5, 600 mM NaCl) and loaded onto an Ni-NTA column to obtain His<sub>6</sub>-tag-removed AfNMT solution as the flow-through.

The protein sample was then diluted fivefold with buffer A (10 mM potassium phosphate pH 7.2, 25 mM NaCl, 1 mM magnesium chloride, 1 mM DTT) and *S*-(2-oxo)pentadecyl-CoA solution was added to a final concentration of 0.3 mM. Next, this sample was loaded onto a hydroxyapatite column (Macro-Prep Ceramic Hydroxyapatite type 1 40 µm, Bio-Rad). After a gradient of buffer B (250 mM potassium phosphate,

25 mM NaCl, 1 mM TCEP pH 7.2) from 0 to 40%, AfNMT fractions were eluted with 40% buffer B. These AfNMT-containing fractions were collected and concentrated to 7.5 ml. This eluted sample was then applied onto Superdex 75 16/60 (GE Healthcare) and eluted with elution buffer [20 mM HEPES pH 7.5, 30 mM NaCl, 1 mM TCEP, 1 µM *S*-(2-oxo)pentadecyl-CoA]. AfNMT-containing fractions were collected and concentrated to 19.7 mg ml<sup>-1</sup>.

#### 2.4. Crystallization and structure determination

*S*-(2-Oxo)pentadecyl-CoA was added to 50 µl protein sample to a final concentration of 0.25 mM. After centrifugation (13 000 rev min<sup>-1</sup>, 10 min, 277 K), the supernatant was subjected to crystallographic analysis. AfNMT crystals were grown at 277 K by the sitting-drop

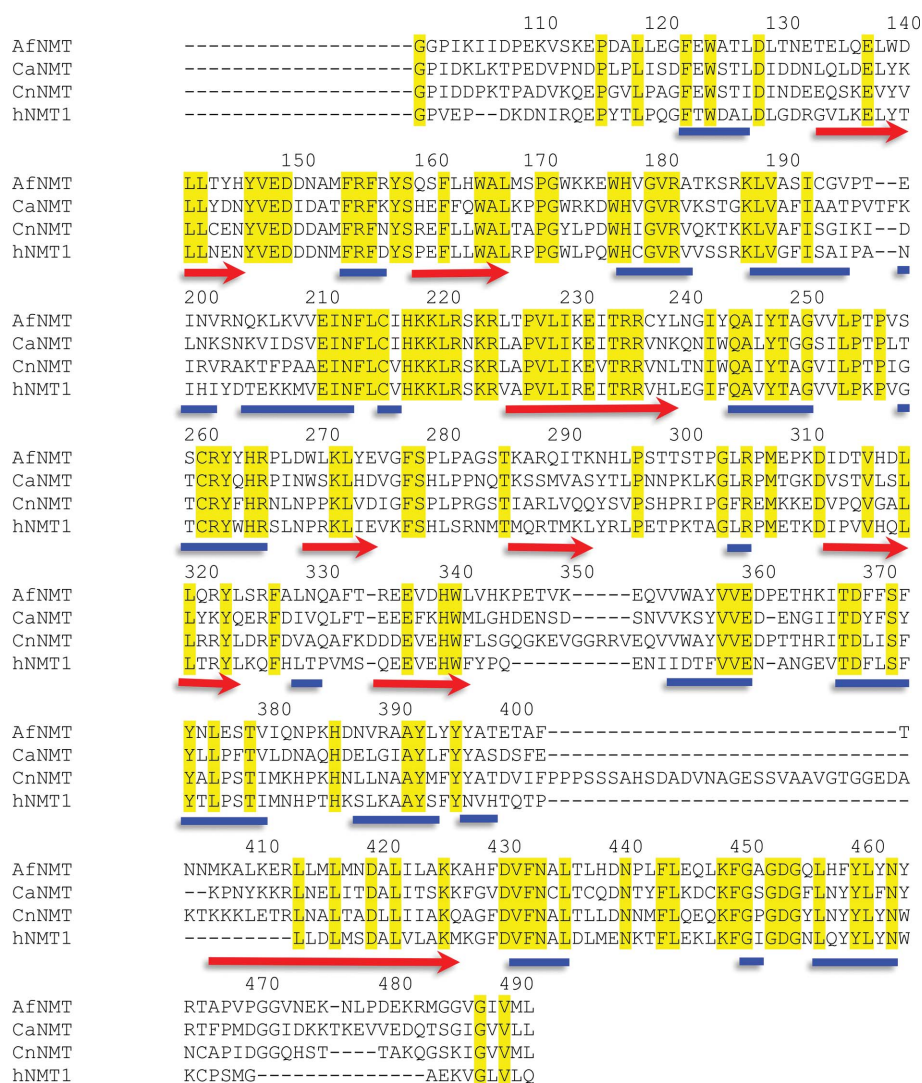


**Figure 2** Amino-acid sequence alignment of NMTs from various species. AfNMT, *Aspergillus fumigatus* NMT (GenBank accession No. BAA87865); CaNMT, *Candida albicans* NMT (GenBank accession No. AAA34351); CnNMT, *Cryptococcus neoformans* NMT (GenBank accession No. AAA17547); hNMT1, human NMT1 (GenBank accession No. AAH06538). The red arrows indicate  $\alpha$ -helical regions and the blue lines indicate  $\beta$ -strand regions. Sequence alignment was performed with *ClustalW* v.1.83.

**Table 1**  
Data-collection conditions and data-processing and refinement statistics.

Values in parentheses are for the outer shell.

|                                       |                                    |
|---------------------------------------|------------------------------------|
| Data-collection conditions            |                                    |
| X-ray source                          | RU-H3C [Cu $K\alpha$ ]             |
| Detector                              | R-Axis IIC                         |
| Wavelength ( $\text{\AA}$ )           | 1.542                              |
| Tube current (kV)                     | 40                                 |
| Voltage (mA)                          | 40                                 |
| Camera length (mm)                    | 91                                 |
| Temperature                           | Room temperature                   |
| Crystal size (mm)                     | 0.15 $\times$ 0.15 $\times$ 0.3    |
| Oscillation range ( $^\circ$ )        | 90                                 |
| $\Delta\phi$ ( $^\circ$ )             | 1.0                                |
| Exposure time (min)                   | 15                                 |
| Data-processing statistics            |                                    |
| Program                               | <i>CrystalClear</i>                |
| Space group                           | $P2_12_12_1$                       |
| Unit-cell parameters ( $\text{\AA}$ ) | $a = 54.79, b = 77.07, c = 113.24$ |
| Spacing ( $\text{\AA}$ )              | 2.1                                |
| Cutoff                                | None                               |
| Completeness (%)                      | 99.7 (99.4)                        |
| $R_{\text{merge}}(I)$ (%)             | 6.40 (28.6)                        |
| Refinement statistics                 |                                    |
| Program                               | <i>REFMAC5</i>                     |
| Resolution range ( $\text{\AA}$ )     | 25–2.10 (2.07–2.10)                |
| No. of reflections                    |                                    |
| Working set                           | 27148                              |
| Free set                              | 1412                               |
| $R$ factor                            | 0.179                              |
| Free $R$ factor                       | 0.217                              |
| Ramachandran plot, residues in (%)    |                                    |
| Most favoured region                  | 96.21                              |
| Allowed region                        | 3.28                               |
| Disallowed region                     | 0.25                               |
| PDB code                              | 4qbj                               |

vapour-diffusion method with a reservoir solution consisting of 1.85–2.3 *M* ammonium sulfate, 0.1 *mM* HEPES pH 7.4, 20 *mM* manganese chloride, 1 *mM* TCEP. The crystals grew as columnar prisms.

To obtain crystals of the ternary AfNMT–*S*-(2-oxo)pentadecyl-CoA–Ro-09-4879 complex, an AfNMT–*S*-(2-oxo)pentadecyl-CoA–Ro-09-4879 solution at a



**Figure 3**  
Overall structure of AfNMT complexed with Ro-09-4879 and *S*-(2-oxo)pentadecyl-CoA. Magenta C atoms, Ro-09-4879; green C atoms, *S*-(2-oxo)pentadecyl-CoA.

decyl-CoA crystal was soaked in Ro-09-4879 solution at a final concentration of 5 *mM* and left at 277 K for two weeks. 30  $\mu\text{l}$  of cryosolution (100 *mM* HEPES pH 7.0, 2.4 *M* ammonium sulfate, 20 *mM* manganese chloride, 1 *mM* TCEP, 20% glycerol) was added to 1  $\mu\text{l}$  of crystal-containing drop and this solution was immediately cooled in liquid nitrogen.

X-ray diffraction data were collected using an in-house R-Axis IIC detector (Rigaku) and were processed and scaled with *CrystalClear* (Pflugrath, 1999). The diffraction data statistics are shown in Table 1. Molecular replacement was performed with *MOLREP* from the *CCP4* package v.4.2.2 (Winn *et al.*, 2011) using the previously solved crystal structure of yeast NMT (PDB entry 1iic; Farazi *et al.*, 2001) as a search model. After replacing the residues of yeast NMT with those of AfNMT, the AfNMT model was built and optimized with *CNX* (v.2000; Accelrys Software Inc., San Diego, California, USA; Brünger *et al.*, 1998) and *REFMAC5* (Murshudov *et al.*, 2011). All figures showing the molecular model were generated with *Maestro* v.10.0 (Schrodinger, New York, USA).

The coordinates of the AfNMT–*S*-(2-oxo)pentadecyl-CoA–Ro-09-4879 crystal structure have been deposited in the RCSB Protein Data Bank under accession code 4qbj.

### 3. Results and discussion

#### 3.1. Crystallization

When we started this study, no crystal structures of AfNMT were known. Therefore, we designed three constructs of AfNMT by comparing the AfNMT amino-acid sequence with the sequence of CaNMT used in crystallization (Weston *et al.*, 1998; Sogabe *et al.*, 2002): (i) full length, (ii) a deletion mutant of the N-terminal 78 residues and (iii) a deletion mutant of the N-terminal 100 residues. After purification of the protein samples, these three constructs each showed a single band on SDS–PAGE (data not shown). However, crystals could only be grown for construct (iii) and no crystals were grown for the other two constructs. We performed DLS analyses of protein samples of constructs (i) and (ii), and the results showed that these protein samples formed aggregates with radii of tens of nanometres and therefore no crystals were formed (data not shown). We concluded that in constructs (i) and (ii) the mobility of the N-terminal 100 residues was very high and disrupted the crystallization of the protein samples.

#### 3.2. Overall structure

The overall structure of AfNMT is shown in Fig. 3. A bundle of  $\beta$ -sheets at the centre of the structure and  $\alpha$ -helices surrounding the bundle were observed. This folding was also observed in NMT homologues from other species, such as human, *C. albicans* and *S. cerevisiae*. The cofactor analogue *S*-(2-oxo)pentadecyl-CoA was found to bind at the N-terminal region, and the synthetic inhibitor Ro-09-4879 bound at the substrate-recognition site in the C-terminal region, which was also the same as in CaNMT (Weston *et al.*, 1998; Sogabe *et al.*, 2002). There was one AfNMT molecule per asymmetric unit. Only one residue, Asn405, was in a disallowed region of

the Ramachandran plot. It was distant from the substrate-recognition site and the cofactor-recognition site.

Electron density for Ro-09-4879 was clearly observed for the whole compound (Fig. 4); however, the *B* factors of the trifluorobenzene atoms showed relatively higher values, by 14–22 Å<sup>2</sup>, than the other regions (the average *B* factor was 37.79 Å<sup>2</sup>). This seemed to reflect the looseness of the molecular recognition around the trifluorobenzene moiety, which might lead to a reduction in the inhibitory activity of Ro-09-4879 towards AfNMT compared with CaNMT. Our crystal structure had a high resolution of around 2.1 Å and several water molecules were observed which provided further information about the interaction between Ro-09-4879 and AfNMT and a good opportunity for precise drug design including water-mediated interactions.

In the structure of AfNMT, the His99 side chain of a neighbouring crystal symmetry mate molecule was positioned near the trifluorobenzene moiety of Ro-09-4879 (Fig. 5). His99 did not form a direct interaction with Ro-09-4879; however, attention should be focused on the optimization of the trifluorobenzene moiety of Ro-09-4879.

### 3.3. Interaction between AfNMT and Ro-09-4879

**3.3.1. Benzofuran ring.** Characteristic interactions between the benzofuran ring of Ro-09-4879 and AfNMT are shown in Fig. 5. This ring occupied a hydrophobic pocket formed by the side chains of Tyr263, Tyr393 and Leu436.  $\pi$ - $\pi$  stacking between the benzofuran ring of Ro-09-4879 and the side chain of Tyr263 and T-shaped stacking between the benzofuran ring and the side chain of Tyr393 seemed to play a critical role in molecular recognition. Therefore, the introduction of an electron-withdrawing substituent onto the benzofuran ring might increase the inhibitory activity of this compound by improving this intermolecular stacking. The carbamoyl plane of the Asn434 side chain was parallel to the benzofuran plane;

this also appeared to make the intermolecular interaction even stronger.

The side chain of His265 plays an interesting role in the recognition of Ro-09-0879. The distance between the benzofuran O atom and the His265 side chain and the distance between the His265 side chain and Asn434 OD were 2.95 and 2.84 Å, respectively. From the point of view of the hydrogen-bond network, it was difficult to determine which tautomer/rotamer was correct for the side chains of His265 and Asn434 and which hydrogen-bond network was correct. In any case, we considered that these hydrogen bonds greatly contribute to the gain in binding free energy because hydrogen bonds in a ‘hydrophobic enclosure environment’ are known to contribute to the affinity significantly (Friesner *et al.*, 2006). In fact, this interaction with the His265 side chain was also formed between CaNMT and the peptidic inhibitor SC-58272 (Sogabe *et al.*, 2002), which was one of two common hydrogen bonds in AfNMT–Ro-09-4879 and CaNMT–SC-58272. Another common hydrogen bond was formed between the C-terminal carboxylate of AfNMT or CaNMT and the inhibitor. These two spots were considered to be hotspots in NMT.

All of the residues surrounding the benzofuran ring of Ro-09-4879, such as Tyr263, His265, Tyr393, Asn434 and Leu436, were conserved among AfNMT, CaNMT, human NMT1 and homologues from other species (Fig. 2). Interactions in this pocket can be utilized to acquire a broad antifungal spectrum; however, such interactions seemed to increase the inhibitory activity against human NMTs and cause side effects.

We compared our crystal structure with the crystal structures of other NMTs bound to benzofuran-based inhibitors

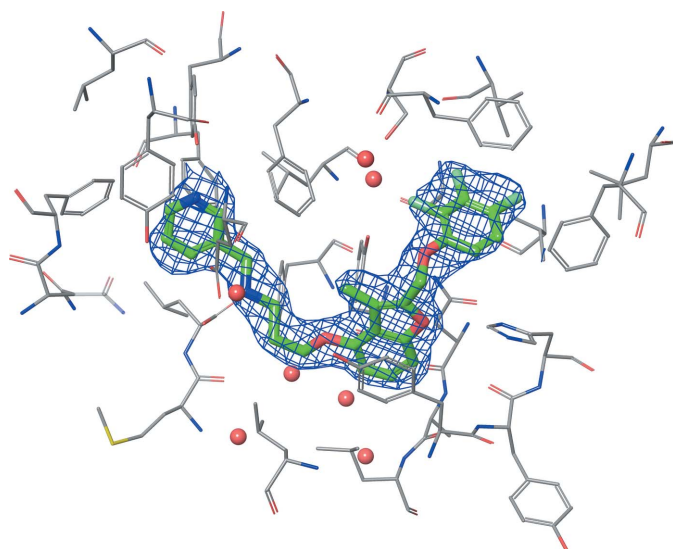


Figure 4  
OMIT electron-density map of Ro-09-4879 (contoured at 1.0 $\sigma$ ).

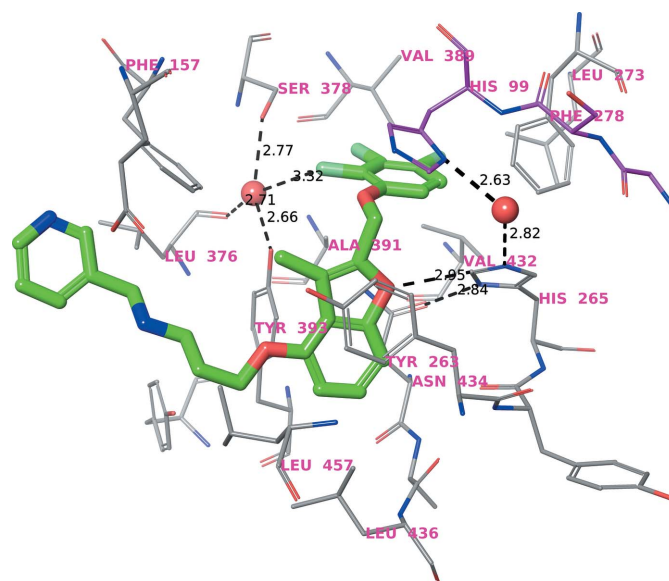


Figure 5  
Intermolecular recognition between AfNMT and Ro-09-4879 around the benzofuran and trifluorobenzene regions. Grey C atoms, AfNMT from the AfNMT–S-(2-oxo)pentadecyl-CoA–Ro-09-4879 complex crystal structure; green C atoms, Ro-09-4879 from the AfNMT crystal structure; magenta C atoms, a crystal symmetry mate of AfNMT; red spheres, water molecules in the AfNMT crystal structure. The black dotted lines indicate probable hydrogen bonds or electrostatic interactions. The numbers in black indicate distances (Å) between two heavy atoms.

(PDB entries 1iyl, 4b11, 4b12, 4b13 and 4b14). A superimposition of our structure with PDB entries 1iyl and 4b14 is shown in Fig. 6 (in PDB entries 4b11, 4b12 and 4b13 the structures of this site were almost the same as in PDB entry 4b14). In our structure, the benzofuran ring occupied a space similar to that in PDB entry 1iyl. On the other hand, in PDB entry 4b14 the benzofuran ring shifted from the position in our structure and in PDB entry 1iyl by about 1.6 Å. As for the surrounding residues, in our structure most residues showed similar positions and rotamers as in PDB entry 1iyl. However, in PDB entry 4b14 the positions and rotamers of some residues such as Phe157, Tyr159 and Tyr263 changed to accommodate the different binding mode of the inhibitor.

**3.3.2. Linker region.** The linker which links the benzofuran ring and pyridine ring of Ro-09-4879 includes an O atom and an N atom. Interactions between these atoms and AfNMT are shown in Fig. 7. The amine N atom in the linker formed a salt bridge with the C-terminal carboxylate of AfNMT and was considered to play a critical role in AfNMT–Ro-09-4879 recognition (Fig. 7). As previously mentioned, this was one of two hotspot interactions which were conserved between AfNMT–Ro-09-4879 and CaNM–SC-58272. This N atom also formed a hydrogen bond to the Glu149 side chain *via* one water molecule (Fig. 7) and the residue was conserved in NMTs from other fungi and the human enzyme (Fig. 2).

**3.3.3. Pyridine ring.** The pyridine ring of Ro-09-4879 seems to contribute to its affinity for AfNMT by forming a stable hydrophobic cluster with the side chains of Tyr147, Phe157, Phe163 and Phe214 (Fig. 7). All of these residues were conserved among most of the species (Fig. 2) and had aromatic rings in their side chains; however, interactions unique to aromatic rings such as  $\pi$ – $\pi$  stacking or T-shaped stacking were not observed in molecular recognition in this area. The hydroxyl of the Tyr159 side chain made a hydrogen bond to

the N atom of the pyridine ring (Fig. 7), which was a ‘hydrogen bond in a hydrophobic enclosure environment’ (Friesner *et al.*, 2006). This interaction seemed to contribute to the binding free energy. However, the protonation of the pyridine ring and the direction of the hydroxyl of the Tyr159 side chain could not be determined from our analysis; therefore, it was uncertain whether the Tyr159 side chain and pyridine N atom act as a hydrogen-bond acceptor or donor. This Tyr159 was also conserved among many species (Fig. 2).

**3.3.4. Trifluorobenzene ring.** A pocket that accommodates the trifluorobenzene moiety of Ro-09-4879 was formed by the side chains of many hydrophobic residues such as Phe155, His265, Phe278, Val389, Ala391 and Val432; however, some hydrophilic residues were also found in this region, such as Ser378 and Asn434 (Fig. 8). The most important residue in the interactions was considered to be Phe155, the side-chain aromatic ring of which adopts a conformation parallel to the trifluorobenzene ring of Ro-09-4879. The three F atoms seemed to make contributions to increase the affinity for AfNMT in three ways. The first was a hydrophobic interaction between the fluorines and surrounding hydrophobic residues. The second was that the fluorine in the *ortho* position forms an indirect hydrogen bond to the hydroxyl group of the Ser378 side chain, the carbonyl of the Leu376 main chain and the hydroxyl of the Tyr393 side chain *via* a structured water molecule (Fig. 8). The hydrogen-bond energy between a fluorine and a hydrogen acceptor atom is considered to be weaker than a typical hydrogen bond (Murray-Rust *et al.*, 1983; Dunitz & Taylor, 1997; Zhou *et al.*, 2009); however, it did contribute to the binding affinity to some extent. The third was the electron-withdrawing effect on the benzene ring, which makes the stacking of the benzene ring and the aromatic ring of the Phe155 side chain stronger.

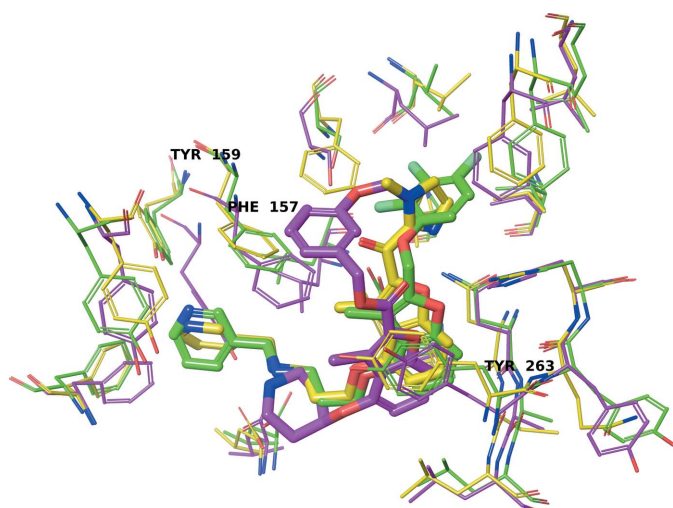


**Figure 6**

Superimposition of crystal structures of NMTs bound to benzofuran-based inhibitors. Green C atoms, AfNMT–S-(2-oxo)pentadecyl-CoA–Ro-09-4879 (bold stick model); yellow C atoms, CaNMT–benzofuran-based inhibitor (bold stick model) complex (PDB entry 1iyl, chain A); magenta C atoms, *P. vivax* NMT–S-(2-oxo)pentadecyl-CoA–benzofuran-based inhibitor (bold stick model) complex (PDB entry 4b14, chain A).

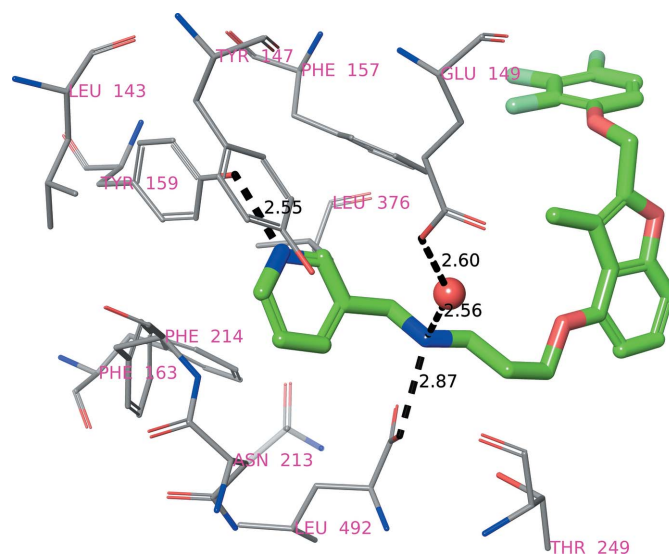


**Figure 7**

Interaction between AfNMT and the pyridine and linker regions of Ro-09-4879. The black dotted lines indicate probable hydrogen bonds. The numbers in black indicate distances (Å) between two heavy atoms.



CoA and the main chain of AfNMT; therefore, the residue differences among species do not affect these interactions. As for the hydrophobic interaction, residue differences were observed among species in many residues forming a hydrophobic cluster, which might contribute to the selectivity of inhibitors. However, the interface of AfNMT with *S*-(2-oxo)pentadecyl-CoA was rather large and therefore it would be difficult to inhibit AfNMT with a small molecule in a competitive manner with the cofactor.

To determine the cofactor-binding site in detail, we tried to obtain cofactor-free crystals. However, *S*-(2-oxo)pentadecyl-CoA-free AfNMT protein samples quickly formed a precipitate in the protein-purification process and we could not obtain pure *S*-(2-oxo)pentadecyl-CoA-free AfNMT crystals (data not shown). This indicated that *S*-(2-oxo)pentadecyl-CoA bound to AfNMT strongly with its large interface and that the binding greatly contributed to the stability of AfNMT. This result also indicated the difficulty of obtaining small-molecule inhibitors that are competitive with the cofactor; therefore, we ceased development of a cofactor-competitive inhibitor.

In this study, we have determined the crystal structure of the tertiary complex of *A. fumigatus* NMT (AfNMT), *S*-(2-oxo)pentadecyl-CoA and Ro-09-4879. The structural information explained the reduced activity of Ro-09-4879 towards *A. fumigatus* compared with *C. albicans*, which is mainly owing to differences in intermolecular recognition in the trifluorobenzene region. This information will allow us to design a novel specific inhibitor of AfNMT.

## Acknowledgements

We thank Dr Hiroyuki Hanzawa for valuable discussions.

## References

- Bhatnagar, R. S., Fütterer, K., Farazi, T. A., Korolev, S., Murray, C. L., Jackson-Machelski, E., Gokel, G. W., Gordon, J. I. & Waksman, G. (1998). *Nature Struct. Biol.* **5**, 1091–1097.
- Boutin, J. A. (1997). *Cell. Signal.* **9**, 15–35.
- Brand, S. *et al.* (2012). *J. Med. Chem.* **55**, 140–152.
- Brannigan, J. A., Roberts, S. M., Bell, A. S., Hutton, J. A., Hodgkinson, M. R., Tate, E. W., Leatherbarrow, R. J., Smith, D. F. & Wilkinson, A. J. (2014). *IUCrJ*, **1**, 250–260.
- Brannigan, J. A., Smith, B. A., Yu, Z., Brzozowski, A. M., Hodgkinson, M. R., Maroof, A., Price, H. P., Meier, F., Leatherbarrow, R. J., Tate, E. W., Smith, D. F. & Wilkinson, A. J. (2010). *J. Mol. Biol.* **396**, 985–999.
- Brünger, A. T., Adams, P. D., Clore, G. M., DeLano, W. L., Gros, P., Grosse-Kunstleve, R. W., Jiang, J.-S., Kuszewski, J., Nilges, M., Pannu, N. S., Read, R. J., Rice, L. M., Simonson, T. & Warren, G. L. (1998). *Acta Cryst.* **D54**, 905–921.
- Chen, S.-H. & Rodriguez, M. (2003). *Drugs Future*, **28**, 441–463.
- Devadas, B., Zupec, M. E., Freeman, S. K., Brown, D. L., Nagarajan, S., Sikorski, J. A., McWherter, C. A., Getman, D. P. & Gordon, J. I. (1995). *J. Med. Chem.* **38**, 1837–1840.
- Dunitz, J. D. & Taylor, R. (1997). *Chem. Eur. J.* **3**, 89–98.
- Ebara, S., Naito, H., Nakazawa, K., Ishii, F. & Nakamura, M. (2005). *Biol. Pharm. Bull.* **28**, 591–595.
- Ebiike, H., Masubuchi, M., Liu, P., Kawasaki, K., Morikami, K., Sogabe, S., Hayase, M., Fujii, T., Sakata, K., Shindoh, H., Shiratori, Y., Aoki, Y., Ohtsuka, T. & Shimma, N. (2002). *Bioorg. Med. Chem. Lett.* **12**, 607–610.
- Farazi, T. A., Waksman, G. & Gordon, J. I. (2001). *Biochemistry*, **40**, 6335–6343.
- Frearson, J. A. *et al.* (2010). *Nature (London)*, **464**, 728–732.
- Friesner, R. A., Murphy, R. B., Repasky, M. P., Frye, L. L., Greenwood, J. R., Halgren, T. A., Sanschagrin, P. C. & Mainz, D. T. (2006). *J. Med. Chem.* **49**, 6177–6196.
- Goncalves, V., Brannigan, J. A., Whalley, D., Ansell, K. H., Saxty, B., Holder, A. A., Wilkinson, A. J., Tate, E. W. & Leatherbarrow, R. J. (2012). *J. Med. Chem.* **55**, 3578–3582.
- Herbrecht, R. *et al.* (2002). *N. Engl. J. Med.* **347**, 408–415.
- Howard, S. J., Pasqualotto, A. C. & Denning, D. W. (2010). *Clin. Microbiol. Infect.* **16**, 683–688.
- Johnson, D. R., Bhatnagar, R. S., Knoll, L. J. & Gordon, J. I. (1994). *Annu. Rev. Biochem.* **63**, 869–914.
- Kawasaki, K., Masubuchi, M., Morikami, K., Sogabe, S., Aoyama, T., Ebiike, H., Niizuma, S., Hayase, M., Fujii, T., Sakata, K., Shindoh, H., Shiratori, Y., Aoki, Y., Ohtsuka, T. & Shimma, N. (2003). *Bioorg. Med. Chem. Lett.* **13**, 87–91.
- Knoll, L. J., Johnson, D. R., Bryant, M. L. & Gordon, J. I. (1995). *Methods Enzymol.* **250**, 405–435.
- Laczowski, K. Z., Misiura, K., Biernasiuk, A., Malm, A., Siwek, A. & Plech, T. (2013). *Lett. Drug. Des. Discov.* **10**, 798–807.
- Latgé, J.-P. (1999). *Clin. Microbiol. Rev.* **12**, 310–350.
- Masubuchi, M., Ebiike, H., Kawasaki, K., Sogabe, S., Morikami, K., Shiratori, Y., Tsujii, S., Fujii, T., Sakata, K., Hayase, M., Shindoh, H., Aoki, Y., Ohtsuka, T. & Shimma, N. (2003). *Bioorg. Med. Chem.* **11**, 4463–4478.
- Masubuchi, M., Kawasaki, K., Ebiike, H., Ikeda, Y., Tsujii, S., Sogabe, S., Fujii, T., Sakata, K., Shiratori, Y., Aoki, Y., Ohtsuka, T. & Shimma, N. (2001). *Bioorg. Med. Chem. Lett.* **11**, 1833–1837.
- Murray-Rust, P., Stallings, W. C., Monti, C. T., Preston, R. K. & Glusker, J. P. (1983). *J. Am. Chem. Soc.* **105**, 3206–3214.
- Murshudov, G. N., Skubák, P., Lebedev, A. A., Pannu, N. S., Steiner, R. A., Nicholls, R. A., Winn, M. D., Long, F. & Vagin, A. A. (2011). *Acta Cryst.* **D67**, 355–367.
- Nakayama, H., Mio, T., Nagahashi, S., Kokado, M., Arisawa, M. & Aoki, Y. (2000). *Infect. Immun.* **68**, 6712–6719.
- Pfaller, A. P., Pappa, P. G. & Wingard, J. R. (2006). *Clin. Infect. Dis.* **43**, S3–S14.
- Pflugrath, J. W. (1999). *Acta Cryst.* **D55**, 1718–1725.
- Rackham, M. D., Brannigan, J. A., Moss, D. K., Yu, Z., Wilkinson, A. J., Holder, A. A., Tate, E. W. & Leatherbarrow, R. J. (2013). *J. Med. Chem.* **56**, 371–375.
- Rudnick, D. A., McWherter, C. A., Gokel, G. W. & Gordon, J. I. (1993). *Adv. Enzymol. Relat. Areas Mol. Biol.* **67**, 375–430.
- Siwek, A., Stefańska, J., Dzitko, K. & Ruszczak, A. (2012). *J. Mol. Model.* **18**, 4159–4170.
- Snelders, E., Melchers, W. J. & Verweij, P. E. (2011). *Future Microbiol.* **6**, 335–347.
- Sogabe, S., Masubuchi, M., Sakata, K., Fukami, T. A., Morikami, K., Shiratori, Y., Ebiike, H., Kawasaki, K., Aoki, Y., Shimma, N., D'Arcy, A., Winkler, F. K., Banner, D. W. & Ohtsuka, T. (2002). *Chem. Biol.* **9**, 1119–1128.
- Weston, S. A., Camble, R., Colls, J., Rosenbrock, G., Taylor, I., Egerton, M., Tucker, A. D., Tunnicliffe, A., Mistry, A., Mancía, F., de la Fortelle, E., Irwin, J., Bricogne, G. & Pauptit, R. A. (1998). *Nature Struct. Biol.* **5**, 213–221.
- Winn, M. D. *et al.* (2011). *Acta Cryst.* **D67**, 235–242.
- Wright, M. H. *et al.* (2014). *Nature Chem.* **6**, 112–121.
- Wu, J., Tao, Y., Zhang, M., Howard, M. H., Gutteridge, S. & Ding, J. (2007). *J. Biol. Chem.* **282**, 22185–22194.
- Yu, Z., Brannigan, J. A., Moss, D. K., Brzozowski, A. M., Wilkinson, A. J., Holder, A. A., Tate, E. W. & Leatherbarrow, R. J. (2012). *J. Med. Chem.* **55**, 8879–8890.
- Zhao, C. & Ma, S. (2014). *ChemMedChem*, **9**, 2425–2437.
- Zhou, P., Zou, J., Tian, F. & Shang, Z. (2009). *J. Chem. Inf. Model.* **49**, 2344–2355.